Numer Algor (2011) 57:187–205
DOI 10.1007/s11075-010-9423-8

ORIGINAL PAPER

# Effects of thermal radiation on the boundary layer flow of a Jeffrey fluid over an exponentially stretching surface

**Sohail Nadeem · Shehla Zaheer · Tiegang Fang**

Received: 11 February 2010 / Accepted: 25 August 2010 /
Published online: 10 September 2010


**Abstract** In the present investigation we have analyzed the boundary layer flow of a Jeffrey fluid over an exponentially stretching surface. The effects of thermal radiation are carried out for two cases of heat transfer analysis known as (1) Prescribed exponential order surface temperature (PEST) and (2) Prescribed exponential order heat flux (PEHF). The highly nonlinear coupled partial differential equations of Jeffrey fluid flow along with the energy equation are simplified by using similarity transformation techniques based on boundary layer assumptions. The reduced similarity equations are then solved analytically by the homotopy analysis method (HAM). The convergence of the HAM series solution is obtained by plotting $\hbar$-curves for velocity and temperature. The effects of physical parameters on the velocity and temperature profiles are examined by plotting graphs.

**Keywords** Jeffrey fluid · Porous stretching surface · Thermal radiations · Boundary layer flow · Series solutions

## 1 Introduction

Recently, interest in boundary layer flow and heat transfer over a stretching sheet has gained considerable attention because of its application in industry and manufacturing processes. Such applications include polymer extrusion,

S. Nadeem (✉) · S. Zaheer
Department of Mathematics, Quaid-i-Azam University 45320, Islamabad 44000, Pakistan
e-mail: snqau@hotmail.com

T. Fang
Mechanical and Aerospace Engineering Department, North Carolina State University,
3182 Broughton Hall-Campus Box 7910, 2601 Stinson Drive, Raleigh, NC 27695, USA

drawing of copper wires, continuous stretching of plastic films and artificial fibers, hot rolling, wire drawing, glass fiber, metal extrusion and metal spinning. A large number of researchers are engaged with this rich area. Liu [1] studied the flow and heat transfer of an electrically conducting fluid of second grade over a stretching sheet subject to a transverse magnetic field. Non-Newtonian magnetohydrodynamic flow over a stretching surface with heat and mass transfer was analyzed by Abel et al. [2]. Khan et al. [3] considered the viscoelastic MHD flow, heat and mass transfer over a porous stretching sheet with dissipation energy and stress work. The effects of viscous dissipation and work done by deformation on the MHD flow and heat transfer of a viscoelastic fluid over a stretching sheet were discussed by Cortell [4]. Liu and Anderson [5] studied the heat transfer in a liquid film on an unsteady stretching sheet. The effects of variable fluid properties and thermocapillarity on the flow of a thin film on an unsteady stretching sheet were studied by Dandapat et al. [6]. Some other relevant studies are cited in [7–12].

In the studies mentioned above simple stretching has been used. There are few attempts in which nonstandard stretching is used, known as exponential stretching. Sajid and Hayat [13] considered the influence of thermal radiation on the boundary layer flow due to an exponentially stretching sheet. Heat and mass transfer in a viscoelastic boundary layer flow over an exponentially stretching sheet were investigated by Sanjayanand and Khan [14]. In another study, Khan and Sanjayanand [15] analyzed the viscoelastic boundary layer flow and heat transfer over an exponentially stretching sheet. Heat and mass transfer in the boundary layer on an exponentially stretching continuous surface have been considered by Magyari and Keller [16].

Motivated by the above analyses, the objective of the present investigation is to study the flow and heat transfer of a Jeffrey fluid over an exponentially stretching sheet. The governing equations of a Jeffrey fluid have been simplified by using suitable similarity transformations and then solved analytically by the HAM technique [17–27] for the two cases of heat transfer configurations known as (1) Prescribed exponential order surface temperature (PEST) and (2) Prescribed exponential order heat flux (PEHF). The convergence of the solutions have been discussed by plotting $\hbar$-curves. The effects of pertinent parameters of Jeffrey fluid model on the flow and heat transfer characteristics are discussed and shown pictorially.

## 2 Formulation of the problem

Consider a steady two dimensional flow of an incompressible Jeffrey fluid over an exponentially stretching surface. We are considering Cartesian coordinate system in such a way that $x$-axis is taken along the stretching surface in the direction of the motion and y-axis is normal to it. The plate is stretched in the x-direction with a velocity $U_w = U_0 \exp(x/l)$ defined at $y = 0$. The flow and heat transfer characteristics under the boundary layer approximations with the radiation effects are governed by the following equations

$$\frac{\partial u}{\partial x}+\frac{\partial v}{\partial y}=0, \tag{1}$$

$$\begin{aligned} u\frac{\partial u}{\partial x}+v\frac{\partial u}{\partial y} &= \frac{\gamma}{1+\lambda_1}\frac{\partial^2 u}{\partial y^2} \\ &\quad + \frac{\gamma\lambda_2}{1+\lambda_1}\left[u\frac{\partial^3 u}{\partial x\partial y^2}+v\frac{\partial^3 u}{\partial y^3}+\frac{\partial u}{\partial y}\frac{\partial^2 u}{\partial x\partial y}-\frac{\partial u}{\partial x}\frac{\partial^2 u}{\partial y^2}\right], \end{aligned} \tag{2}$$

$$\begin{aligned} u\frac{\partial T}{\partial x}+v\frac{\partial T}{\partial y} &= \alpha\frac{\partial^2 T}{\partial y^2}+\frac{\gamma}{c_p(1+\lambda_1)}\left(\frac{\partial u}{\partial y}\right)^2 \\ &\quad + \frac{\gamma\lambda_2}{c_p(1+\lambda_1)}\frac{\partial u}{\partial y}\frac{\partial}{\partial y}\left(u\frac{\partial u}{\partial x}+v\frac{\partial u}{\partial y}\right)-\frac{1}{\rho c_p}\frac{\partial q_r}{\partial y}, \end{aligned} \tag{3}$$

where $(u, v)$ are the velocity components in $(x, y)$ directions, $\rho$ is the fluid density, $\gamma$ is the kinematic viscosity, $T$ is the fluid temperature, $\lambda_1$ is the ratio of relaxation to retardation time, $\lambda_2$ is the retardation time, $\alpha$ is the thermal diffusivity, $c_p$ is the specific heat and $q_r$ is the radiative heat flux. The corresponding boundary conditions for the flow problem are

$$\begin{aligned} &u=U_w(x)=U_0\exp\left(\frac{x}{l}\right), \quad v=-\beta(x), \quad T=T_w, \quad at\ y=0, \\ &u=0, \quad u_y=0, \quad T=T_\infty \quad as\ y\to\infty, \end{aligned} \tag{4}$$

in which $U_0$ is the reference velocity, $\beta(x)$ is the suction velocity when $\beta(x)>0$ and $\beta(x)<0$ for mass injection, $T_w$ and $T_\infty$ are the temperatures of the sheet and the ambient fluid respectively. Using the Rosseland approximation of radiation, we can write [28]

$$q_r=-\frac{4\sigma*}{3k*}\frac{\partial T^4}{\partial y}. \tag{5}$$

In the above equation $\sigma^*$ is the Stefan–Boltzmann constant, $k^*$ is the absorption coefficient and by Taylor's series we can write

$$T^4=4T_\infty^3 T-3T_\infty^4. \tag{6}$$

Making use of (5) and (6), (3) can be written as

$$\begin{aligned} u\frac{\partial T}{\partial x}+v\frac{\partial T}{\partial y} &= \left(\alpha+\frac{16\sigma^* T_\infty^3}{3k^*\rho c_p}\right)\frac{\partial^2 T}{\partial y^2}+\frac{\gamma}{c_p(1+\lambda_1)}\left(\frac{\partial u}{\partial y}\right)^2 \\ &\quad + \frac{\gamma\lambda_2}{c_p(1+\lambda_1)}\frac{\partial u}{\partial y}\frac{\partial}{\partial y}\left(u\frac{\partial u}{\partial x}+v\frac{\partial u}{\partial y}\right). \end{aligned} \tag{7}$$

We are interested to consider two types of heat transfer problems defined as

1. The prescribed exponential order surface temperature (PEST)
2. The prescribed exponential order heat flux (PEHF)

The corresponding boundary conditions for the above two cases are defined as

$$T = T_w = T_\infty + T_0 \exp\left(\frac{v_0 x}{2l}\right) \qquad at\ \ y = 0 \text{ for PEST case} \tag{8}$$

$$-k\left(\frac{\partial T}{\partial y}\right)_w = T_1 \exp\left(\frac{v_1+1}{2l}\right) x \qquad at\ \ y = 0 \text{ for PEHF case} \tag{9}$$

and for both the cases

$$T \to T_\infty \quad as\ \ y \to \infty. \tag{10}$$

Here $T_w$ is wall temperature, $v_0$, $v_1$, $T_0$ and $T_1$ are constants.

Introducing the following similarity variables and non-dimensional quantities

$$u = U_0 \exp\left(\frac{x}{l}\right)\ f'(\eta)\,,\ \ v = -\sqrt{\frac{\gamma U_0}{2l}} \exp\left(\frac{x}{2l}\right)\left\{f(\eta) + \eta f'(\eta)\right\},$$

$$\eta = y\sqrt{\frac{U_0}{2\gamma l}} \exp\left(\frac{x}{2l}\right), \tag{11}$$

$$T = T_\infty + T_0 \exp\left(\frac{v_0 x}{2l}\right)\theta(\eta); \qquad \text{for PEST case,} \tag{12}$$

$$T = T_\infty + \frac{T_1}{k}\sqrt{\frac{2\gamma l}{U_0}} \exp\left(\frac{v_1 x}{2l}\right) g(\eta)\,; \qquad \text{for PEHF case.} \tag{13}$$

the resulting problems can be reduced to

$$2(1+\lambda_1)\, f_\eta^2 - (1+\lambda_1)\, ff_{\eta\eta} = f_{\eta\eta\eta} + B\left[f_\eta f_{\eta\eta\eta} - \frac{1}{2} ff_{\eta\eta\eta\eta} + \frac{3}{2} f_{\eta\eta}^2\right], \tag{14}$$

$$f = -v_w,\ f_\eta = 1\ at\ \eta = 0,\ f_\eta = 0\ as\ \eta \to \infty, \tag{15}$$

$$\begin{aligned}(1+\lambda_1)\,\theta_{\eta\eta}\left(1+\frac{4R}{3}\right) &+ (1+\lambda_1)\Pr\left(f\theta_\eta - v_0 f_\eta\theta\right)\\ &= -\Pr E\left[f_{\eta\eta}^2 + \frac{B}{2} f_{\eta\eta}\left\{3 f_{\eta\eta} f_\eta - f_{\eta\eta\eta} f\right\}\right],\end{aligned} \tag{16}$$

$$\theta(0) = 1, \tag{17}$$

$$\theta(\infty) = 0, \tag{18}$$

$$(1+\lambda_1)\, g_{\eta\eta}\left(1+\frac{4R}{3}\right)+(1+\lambda_1)\Pr\left(fg_\eta - v_1 f_\eta g\right)$$
$$= -\Pr E\left[f_{\eta\eta}^2+\frac{B}{2}f_{\eta\eta}\left\{3f_{\eta\eta}f_\eta - f_{\eta\eta\eta}f\right\}\right], \tag{19}$$

$$g_\eta(0) = -1, \tag{20}$$

$$g(\infty) = 0. \tag{21}$$

In the above equations $f$ is the dimensionless stream function, $B = \frac{\lambda_2 U_0 \exp\left(\frac{x}{l}\right)}{l}$ is a local dimensionless parameter and $v_w$ is the dimensionless local suction and injection parameter with $v_w < 0$ for suction and $v_w > 0$ for injection, $\Pr = \gamma/\alpha$ is the Prandtl number, $\left(E = \frac{U_0^2}{c_p T_0}\left(\frac{U_w}{U_0}\right)^{\left(\frac{4-v_0}{2}\right)}\right)$, $\left(E = \frac{kU_0^2}{c_p T_1\sqrt{\frac{2\gamma l}{U_0}}}\left(\frac{U_w}{U_0}\right)^{\left(\frac{4-v_1}{2}\right)}\right)$ are the respective local Eckert numbers for both the cases and $R = \frac{4\sigma^* T_\infty^3}{kk^*}$ is the radiation parameter. Based on the definition for $v_w$, it is obtained that $\beta(x) = -v_w\sqrt{\frac{\gamma U_0}{2l}}\exp\left(\frac{x}{2l}\right)$. Strictly speaking, since $B$ depends on $x$, the resultant ordinary differential equations are not pure similarity equations for the whole flow domain. However, these equations represent local similarity for any given values of $x$. The physical quantities of interest in this problem are the local skin-friction coefficient and the local Nusselt number. The dimensionless local skin-friction coefficient is expressed as

$$C_{f_x} = \frac{\tau_w|_{y=0}}{\rho U_0^2 e^{\frac{2x}{l}}}, \tag{22}$$

where $\tau_w$ is the shear stress at the wall. In terms of dimensionless variables, we have

$$\sqrt{2\mathrm{Re}}C_{f_x} = \frac{1}{1+\lambda_1}\left[f''(0)+\frac{B}{2}\left\{3f''(0)+v_w f'''(0)\right\}\right], \tag{23}$$

where $\mathrm{Re} = \frac{U_w l}{\gamma}$ is the Reynolds number. The local Nusselt number for the PEST case can be written as

$$Nu_x = -\frac{x}{T_w - T_\infty}\left(1+\frac{4R}{3}\right)\left.\frac{\partial T}{\partial y}\right|_{y=0}. \tag{24}$$

Substituting (12) in (24) we obtain

$$Nu_x/\sqrt{\mathrm{Re}_x} = -\sqrt{\frac{x}{2l}}\left(1+\frac{4R}{3}\right)\theta'(0), \tag{25}$$

where $\mathrm{Re}_x = \frac{U_w x}{\gamma}$ is the local Reynolds number.

## 3 Solution by homotopy analysis method

For flow and both PEST and PEHF cases of the heat transfer problem, the initial guesses and the linear operators $L_i\,(i = 1 - 3)$ are

$$f_0(\eta) = 1 - v_w - e^{-\eta}, \quad \theta_0(\eta) = e^{-\eta}, \quad g_0(\eta) = e^{-\eta}, \tag{26}$$

$$\mathrm{L}(f) = f''' - f', \quad \mathrm{L} = f'' - f, \quad \mathrm{L} = f'' - f. \tag{27}$$

The operators satisfy the following properties

$$\mathrm{L}\left[C_1 e^{-\eta} + C_2 e^{\eta} + C_3\right] = 0, \tag{28}$$

$$\mathrm{L}\left[C_4 e^{-\eta} + C_5 e^{\eta}\right] = 0, \tag{29}$$

$$\mathrm{L}\left[C_6 e^{-\eta} + C_7 e^{\eta}\right] = 0, \tag{30}$$

in which $C_1$ to $C_7$ are constants. From (14), (16) and (19) we can define the following zeroth-order deformation problems

$$(1-p)\,\mathrm{L}\left[\hat{f}(\eta,\,p) - f_0(\eta)\right] = p\hbar_1 H_1 \tilde{N}_1\left[\hat{f}(\eta,\,p)\right], \tag{31}$$

$$(1-p)\,\mathrm{L}\left[\hat{\theta}(\eta,\,p) - \theta_0(\eta)\right] = p\hbar_2 H_2 \tilde{N}_2\left[\hat{\theta}(\eta,\,p)\right], \tag{32}$$

$$(1-p)\,\mathrm{L}\left[\hat{g}(\eta,\,p) - g_0(\eta)\right] = p\hbar_3 H_3 \tilde{N}_3\left[\hat{g}(\eta,\,p)\right], \tag{33}$$

$$\hat{f}(0,\,p) = -v_w, \quad \hat{f}'(0,\,p) = 1, \quad \hat{f}'(\infty,\,p) = 0, \tag{34}$$

$$\hat{\theta}(0,\,p) = 1, \quad \hat{\theta}(\infty,\,p) = 0, \tag{35}$$

$$\hat{g}'(0,\,p) = -1, \quad \hat{g}(\infty,\,p) = 0. \tag{36}$$

In (31) to (33), $\hbar_1$, $\hbar_2$ and $\hbar_3$ denote the non-zero auxiliary parameters, $H_1$, $H_2$ and $H_3$ are the non-zero auxiliary functions and

$$\tilde{N}_1\left[\hat{f}(\eta,\,p)\right] = \frac{\partial^3 f}{\partial\eta^3} - 2(1+\lambda_1)\left(\frac{\partial f}{\partial\eta}\right)^2 + (1+\lambda_1) f\frac{\partial^2 f}{\partial\eta^2} + B\left[\frac{\partial f}{\partial\eta}\frac{\partial^3 f}{\partial\eta^3} - \frac{1}{2} f\frac{\partial^4 f}{\partial\eta^4} + \frac{3}{2}\left(\frac{\partial^2 f}{\partial\eta^2}\right)^2\right], \tag{37}$$

$$\tilde{N}_2\left[\hat{\theta}(\eta,\ p)\right] = (1+\lambda_1)\ \frac{\partial^2\theta}{\partial\eta^2}\left(1+\frac{4R}{3}\right) + (1+\lambda_1)\ \Pr\left(f\frac{\partial\theta}{\partial\eta} - v_0\frac{\partial f}{\partial\eta}\theta\right)$$
$$+ \Pr E\left[\left(\frac{\partial^2 f}{\partial\eta^2}\right)^2 + \frac{B}{2}\frac{\partial^2 f}{\partial\eta^2}\left\{3\frac{\partial f}{\partial\eta}\frac{\partial^2 f}{\partial\eta^2} - f\frac{\partial^3 f}{\partial\eta^3}\right\}\right], \tag{38}$$

$$\tilde{N}_3\left[\hat{g}(\eta,\ p)\right] = (1+\lambda_1)\ \frac{\partial^2 g}{\partial\eta^2}\left(1+\frac{4R}{3}\right) + (1+\lambda_1)\ \Pr\left(f\frac{\partial g}{\partial\eta} - v_1\frac{\partial f}{\partial\eta}g\right)$$
$$+ \Pr E\left[\left(\frac{\partial^2 f}{\partial\eta^2}\right)^2 + \frac{B}{2}\frac{\partial^2 f}{\partial\eta^2}\left\{3\frac{\partial f}{\partial\eta}\frac{\partial^2 f}{\partial\eta^2} - f\frac{\partial^3 f}{\partial\eta^3}\right\}\right]. \tag{39}$$

Obviously

$$\hat{f}(\eta,\ 0) = f_0(\eta)\,, \quad \hat{f}(\eta,\ 1) = f(\eta)\,, \tag{40}$$

$$\hat{\theta}(\eta,\ 0) = \theta_0(\eta)\,, \quad \hat{\theta}(\eta,\ 1) = \theta(\eta)\,, \tag{41}$$

$$\hat{g}(\eta,\ 0) = g_0(\eta)\,, \quad \hat{g}(\eta,\ 1) = g(\eta)\,. \tag{42}$$

When $p$ varies from 0 to 1, then $\hat{f}(\eta, p)$, $\hat{\theta}(\eta, p)$, $\hat{g}(\eta, p)$ vary from initial guesses $f_0(\eta)$, $\theta_0(\eta)$ and $g_0(\eta)$ to the final solutions $f(\eta)$, $\theta(\eta)$ and $g(\eta)$ respectively. Considering that the auxiliary parameters $\hbar_1$, $\hbar_2$ and $\hbar_3$ are so properly chosen that the Taylor series of $\hat{f}(\eta, p)$, $\hat{\theta}(\eta, p)$ and $\hat{g}(\eta, p)$ expanded with respect to an embedding parameter converge at $p = 1$. Hence (40) to (42) become

$$\hat{f}(\eta,\ p) = f_0(\eta) + \sum_{m=1}^{\infty} f_m(\eta)\ p^m, \tag{43}$$

$$\hat{\theta}(\eta,\ p) = \theta_0(\eta) + \sum_{m=1}^{\infty} \theta_m(\eta)\ p^m, \tag{44}$$

$$\hat{g}(\eta,\ p) = g_0(\eta) + \sum_{m=1}^{\infty} g_m(\eta)\ p^m, \tag{45}$$

$$f_m(\eta) = \frac{1}{m!}\ \left.\frac{\partial^m \hat{f}(\eta,\ p)}{\partial p^m}\right|_{p=0}, \tag{46}$$

$$\theta_m(\eta) = \frac{1}{m!}\ \left.\frac{\partial^m \hat{\theta}(\eta,\ p)}{\partial p^m}\right|_{p=0}, \tag{47}$$

$$g_m(\eta) = \frac{1}{m!} \left. \frac{\partial^m \hat{g}(\eta,\ p)}{\partial p^m} \right|_{p=0}. \tag{48}$$

The $m$th order problems are defined as follow

$$\mathrm{L}\left[f_m(\eta) - \chi_m f_{m-1}(\eta)\right] = \hbar_1 R_m^1(\eta), \tag{49}$$

$$\mathrm{L}\left[\theta_m(\eta) - \chi_m \theta_{m-1}(\eta)\right] = \hbar_2 R_m^2(\eta), \tag{50}$$

$$\mathrm{L}\left[g_m(\eta) - \chi_m g_{m-1}(\eta)\right] = \hbar_3 R_m^3(\eta), \tag{51}$$

$$f_m(0) = f_m'(0) = f_m'(\infty) = 0, \tag{52}$$

$$\theta_m(0) = \theta_m(\infty) = 0, \tag{53}$$

$$g_m'(0) = g_m(\infty) = 0, \tag{54}$$

where

$$\chi_m = \begin{cases} 0, & m \leq 1, \\ 1, & m > 1. \end{cases} \tag{55}$$

$$\begin{aligned} R_m^1(\eta) = {} & f_{m-1}'''(\eta) + B \sum_{k=0}^{m-1} \left[ f_{m-1-k}' f_k''' - \frac{1}{2} f_{m-1-k} f_k'''' + \frac{3}{2} f_{m-1-k}'' f_k'' \right] \\ & + (1+\lambda_1) \sum_{k=0}^{m-1} f_{m-1-k} f_k'' - 2(1+\lambda_1) \sum_{k=0}^{m-1} f_{m-1-k}' f_k', \end{aligned} \tag{56}$$

$$\begin{aligned} R_m^2(\eta) = {} & (1+\lambda_1)\, \theta_{m-1}'' \left(1 + \frac{4R}{3}\right) + (1+\lambda_1) \Pr \sum_{k=0}^{m-1} \left\{ f_{m-1-k} \theta_k' - v_0 f_{m-1-k}' \theta_k \right\} \\ & + E \Pr \left[ \sum_{k=0}^{m-1} f_{m-1-k}'' f_k'' + \frac{B}{2} \left\{ 3 \sum_{k=0}^{m-1} f_{m-1-k}'' \sum_{k=0}^{m-1} f_{m-1-k}'' f_k' \right.\right. \\ & \left.\left. - \sum_{k=0}^{m-1} f_{m-1-k}''' \sum_{j=0}^{k} f_j'' f_{k-j}' \right\} \right], \end{aligned} \tag{57}$$

$$R_m^3(\eta) = (1+\lambda_1)\ g''_{m-1}\left(1+\frac{4R}{3}\right) + (1+\lambda_1)\ \Pr\sum_{k=0}^{m-1}\left\{f_{m-1-k}g'_k - v_1 f'_{m-1-k}g_k\right\}$$

$$+ E\Pr\left[\sum_{k=0}^{m-1} f''_{m-1-k}f''_k + \frac{B}{2}\left\{3\sum_{k=0}^{m-1} f''_{m-1-k}\sum_{k=0}^{m-1} f''_{m-1-k}f'_k\right.\right.$$

$$\left.\left. - \sum_{k=0}^{m-1} f'''_{m-1-k}\sum_{j=0}^{k} f''_j f_{k-j}\right\}\right]. \qquad (58)$$

Employing MATHEMATICA, (49) to (54) have the following solutions

$$f(\eta) = \sum_{m=0}^{\infty} f_m(\eta) = \lim_{M\to\infty}\left[\sum_{m=0}^{M} a_{m,0}^0 + \sum_{n=1}^{M+1} e^{-n\eta}\left(\sum_{m=n-1}^{M}\sum_{k=0}^{m+1-n} a_{m,n}^k\eta^k\right)\right], \quad (59)$$

$$\theta(\eta) = \sum_{m=0}^{\infty}\theta_m(\eta) = \lim_{M\to\infty}\left[\sum_{n=1}^{M+2} e^{-n\eta}\left(\sum_{m=n-1}^{M+1}\sum_{k=0}^{m+1-n} A_{m,n}^k\eta^k\right)\right], \quad (60)$$

$$g(\eta) = \sum_{m=0}^{\infty} g_m(\eta) = \lim_{M\to\infty}\left[\sum_{n=1}^{M+2} e^{-n\eta}\left(\sum_{m=n-1}^{M+1}\sum_{k=0}^{m+1-n} F_{m,n}^k\eta^k\right)\right], \quad (61)$$

in which $a_{m,0}^0$, $a_{m,n}^k$, $A_{m,n}^k$, $F_{m,n}^k$ are the constants and the numerical data of above solutions are shown through graphs in the proceeding section.

## 4 Results and discussion

The numerical data of the solutions (58) to (60), which is obtained using Mathematica, are discussed using graphs and tables. The convergence of the series solutions strongly depends on the values of the non-zero auxiliary parameters $\hbar_i (i = 1, 2, 3)$ which can be adjusted to control the convergence of the solutions. Therefore, for the convergence of the solution, the $\hbar_i$-curves are plotted in Figs. 1, 2 and 3 for different physical parameters. The admissible ranges of $\hbar_i$ are $-1.1 \le \hbar_1 \le -0.1$, $-0.9 \le \hbar_2 \le -0.1$, $-0.9 \le \hbar_3 \le -0.1$ respectively. The velocity and temperature profiles for different values of parameters $B$, $\lambda_1$, $v_w$, Pr, $E$ and $R$ are displayed in Figs. 4, 5, 6, 7, 8, 9, 10, 11, 12, 13, 14, 15, 16, 17 and 18. It is observed that the velocity field increases with the increase in $B$ and $v_w$ while it decreases with the increase in $\lambda_1$ Moreover, the boundary layer thickness increases with the increase in $B$ and $v_w$ while decreases with the increase in $\lambda_1$ (see Figs. 4, 5 and 6). The temperature profiles

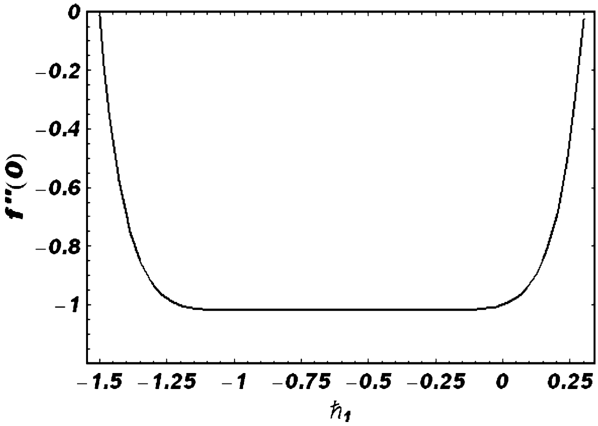


**Fig. 1** $\hbar$-curve for $f(\eta)$ when $\lambda_1 = 0.2$, $B = 0.4$ and $v_w = 0.2$

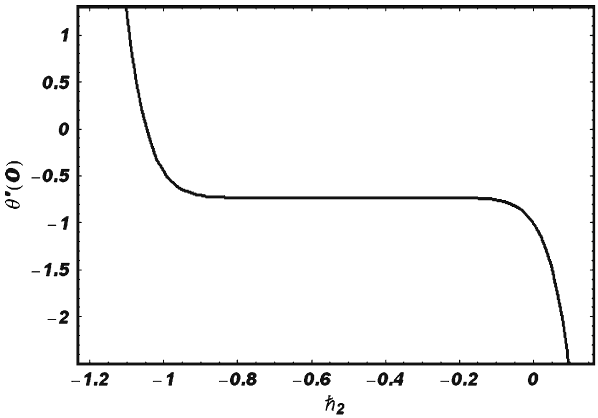


**Fig. 2** $\hbar$-curve for $\theta(\eta)$ in the PEST case when $\hbar_1 = -0.4$, $\lambda_1 = 0.2$, $B = 0.4$, $E = 0.5$, $\mathrm{Pr} = 2$, $R = 0.5$, $v_0 = 1$ and $v_w = 0.2$

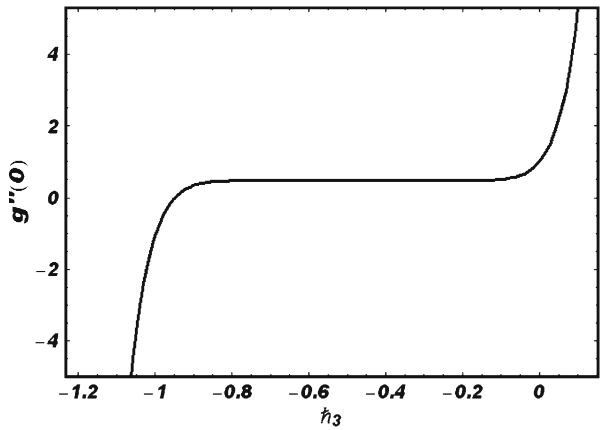


**Fig. 3** $\hbar$-curve for $g(\eta)$ in the PEHF case when $\hbar_1 = -0.4$, $\lambda_1 = 0.2$, $B = 0.4$, $E = 0.5$, $\mathrm{Pr} = 2$, $R = 0.5$, $v_1 = 1$ and $v_w = 0.2$

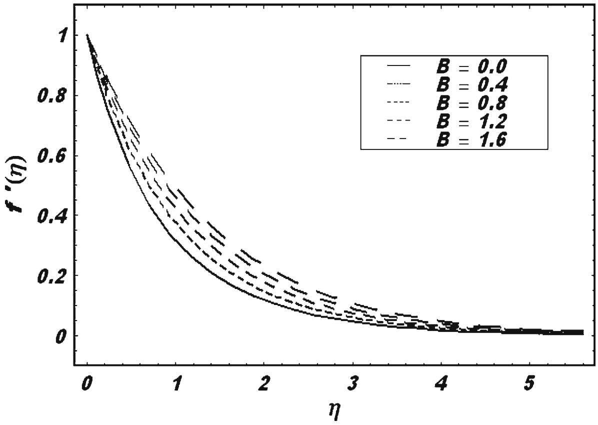


**Fig. 4** Velocity profiles $f'(\eta)$ for different values of $B$ when $\hbar_1 = -0.4$, $\lambda_1 = 0.2$ and $v_w = 0.2$

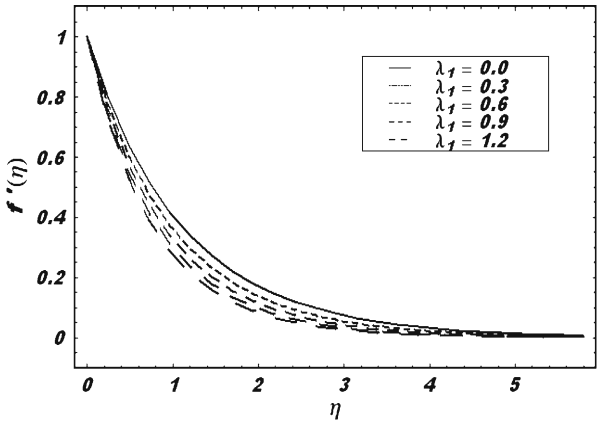


**Fig. 5** Velocity profiles $f'(\eta)$ for different values of $\lambda_1$ when $\hbar_1 = -0.4$, $B = 0.4$ and $v_w = 0.2$

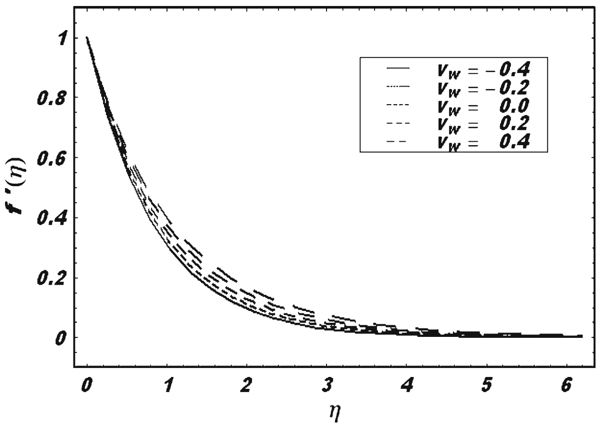


**Fig. 6** Velocity profiles $f'(\eta)$ for different values of $v_w$ when $\hbar_1 = -0.4$, $\lambda_1 = 0.2$ and $B = 0.4$

**Fig. 7** Temperature profiles in the PEST case for different values of $\lambda_1$ when $\hbar_1 = -0.4 = \hbar_2$, $\Pr = 2$, $R = 0.5$, $B = 0.4$, $v_0 = 1$, $v_w = 0.2$ and $E = 0.5$

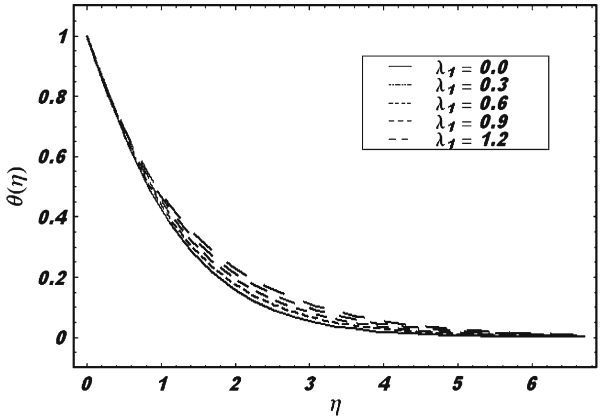


**Fig. 8** Temperature profiles in the PEST case for different values of $B$ when $\hbar_1 = -0.4 = \hbar_2$, $\Pr = 2$, $R = 0.5$, $\lambda_1 = 0.2$, $v_0 = 1$, $v_w = 0.2$ and $E = 0.5$

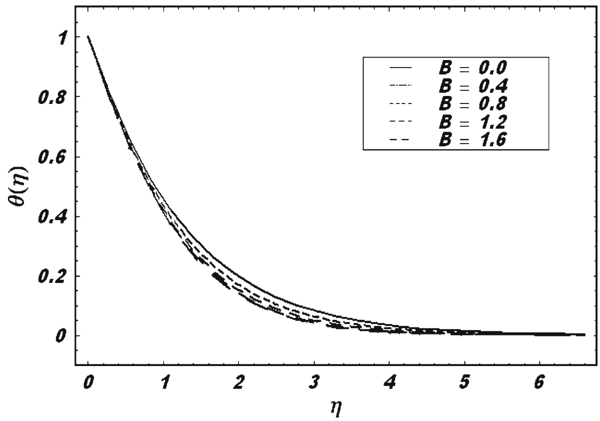


**Fig. 9** Temperature profiles in the PEST case for different values of $v_w$ when $\hbar_1 = -0.4 = \hbar_2$, $\Pr = 2$, $R = 0.5$, $\lambda_1 = 0.2$, $v_0 = 1$, $B = 0.4$ and $E = 0.5$

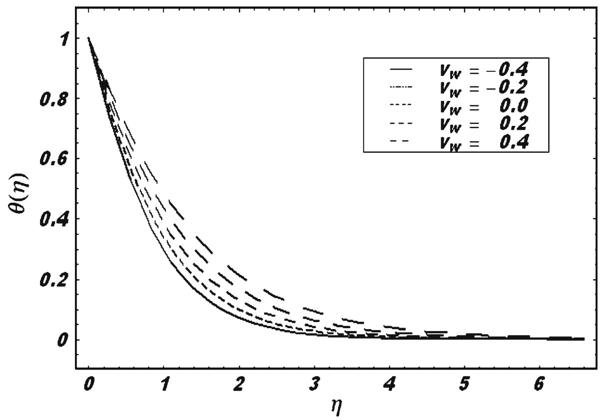

**Fig. 10** Temperature profiles in the PEST case for different values of Pr when $\hbar_1 = -0.4 = \hbar_2$, $B = 0.4$, $R = 0.5$, $v_w = 0.2$, $v_0 = 1$, $E = 0.5$ and $\lambda_1 = 0.2$

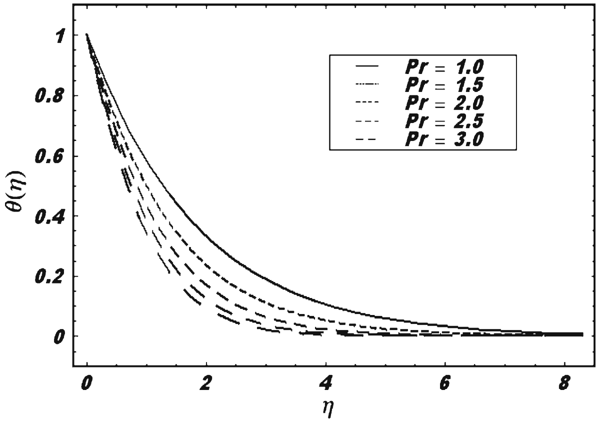


**Fig. 11** Temperature profiles in the PEST case for different values of $E$ when $\hbar_1 = -0.4 = \hbar_2$, Pr $= 2$ $v_0 = 1$, $R = 0.5$, $B = 0.4$, $\lambda_1 = 0.2$ and $v_w = 0.2$

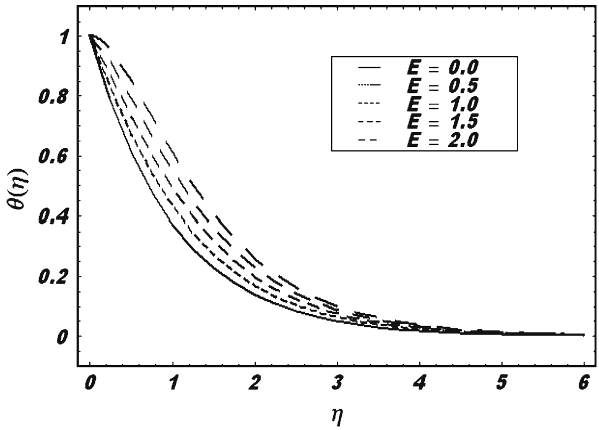


**Fig. 12** Temperature profiles in the PEST case for different values of $R$ when $\hbar_1 = -0.4 = \hbar_2$, Pr $= 2$, $E = 0.5$, $v_w = 0.2$, $B = 0.4$, $\lambda_1 = 0.2$ and $v_0 = 1$

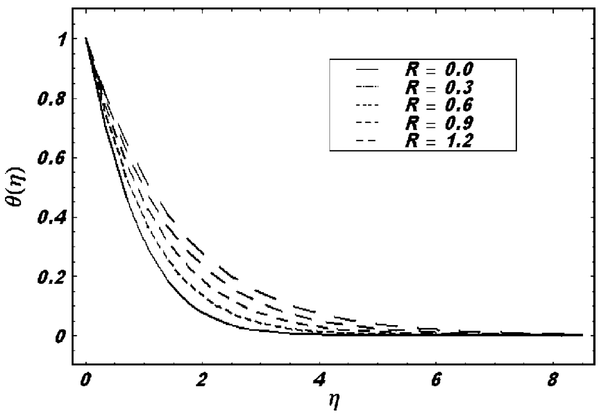

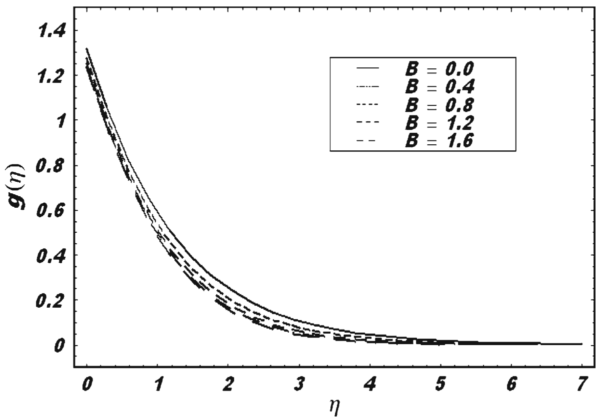


**Fig. 13** Temperature profiles in the PEHF case for different values of $B$ when $\hbar_1 = -0.4 = \hbar_3$, $\Pr = 2$, $R = 0.5$, $v_w = 0.2$, $v_1 = 1$, $E = 0.5$ and $\lambda_1 = 0.2$

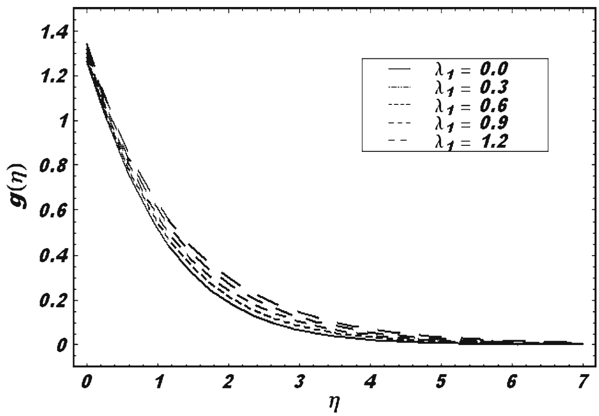


**Fig. 14** Temperature profiles in the PEHF case for different values of $\lambda_1$ when $\hbar_1 = -0.4 = \hbar_3$, $\Pr = 2$, $R = 0.5$, $B = 0.4$, $v_1 = 1$, $v_w = 0.2$ and $E = 0.5$

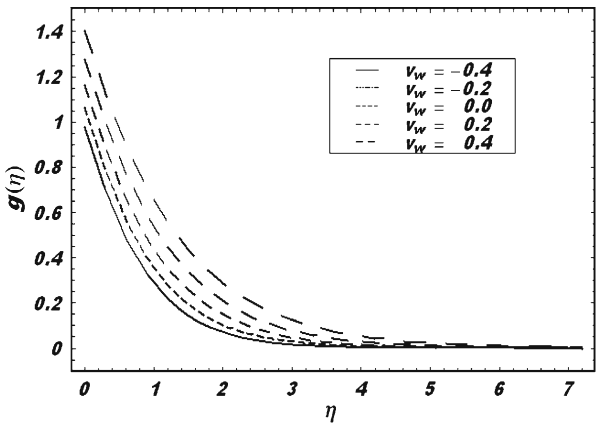


**Fig. 15** Temperature profiles in the PEHF case for different values of $v_w$ when $\hbar_1 = -0.4 = \hbar_3$, $\Pr = 2$, $R = 0.5$, $B = 0.4$, $v_1 = 1$, $E = 0.5$ and $\lambda_1 = 0.2$

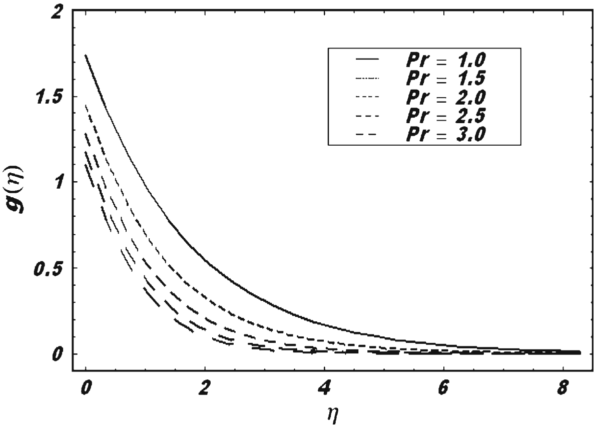


**Fig. 16** Temperature profiles in the PEHF case for different values of Pr when $\hbar_1 = -0.4 = \hbar_3$, $B = 0.4$, $R = 0.5$, $\nu_1 = 1$, $\nu_w = 0.2$, $E = 0.5$ and $\lambda_1 = 0.2$

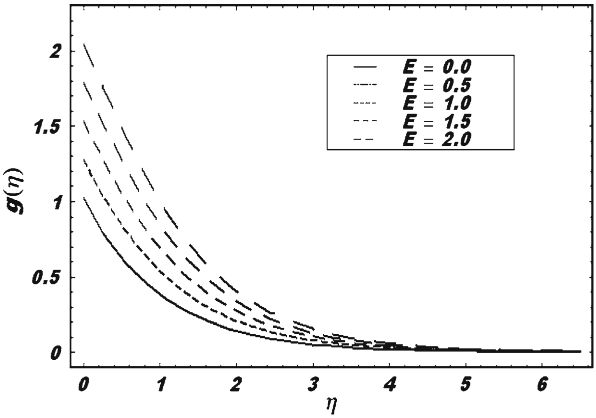


**Fig. 17** Temperature profiles in the PEHF case for different values of $E$ when $\hbar_1 = -0.4 = \hbar_3$, $\mathrm{Pr} = 2$, $R = 0.5$, $B = 0.4$, $\nu_w = 0.2$, $\nu_1 = 1$ and $\lambda_1 = 0.2$

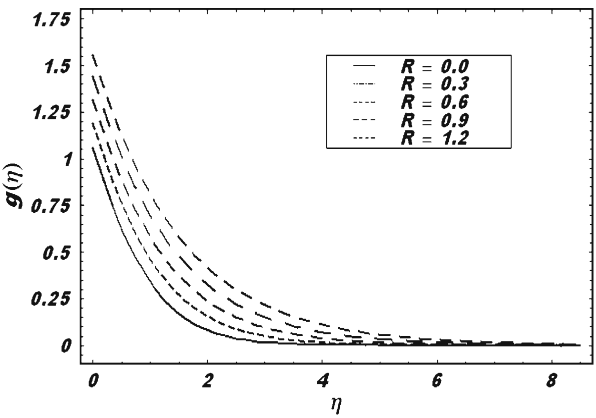


**Fig. 18** Temperature profiles in the PEHF case for different values of $R$ when $\hbar_1 = -0.4 = \hbar_3$, $\mathrm{Pr} = 2$, $\nu_w = 0.2$, $\nu_1 = 1$, $B = 0.4$, $E = 0.5$ and $\lambda_1 = 0.2$

**Table 1** Values of wall temperature gradient $-\theta'(0)$ in the PEST case for different values of $E$, Pr and $R$ keeping $\lambda_1 = 0$, $B = 0$, $v_w = 0$ and $\hbar_1 = \hbar_2 = \hbar$ in comparisons with the results obtained by Bidin and Nazar [28]

| $R$ | Bidin and Nazar [28] | | | Present results (HAM) | | |
|---|---|---|---|---|---|---|
| | $E = 0$ | | | $E = 0$ | | |
| | Pr = 1 | Pr = 2 | Pr = 3 | Pr = 1 ($\hbar = -0.75$) | Pr = 2 ($\hbar = -0.7$) | Pr = 3 ($\hbar = -0.6$) |
| 0 | 0.955 | 1.471 | 1.869 | 0.955 | 1.471 | 1.870 |
| 0.5 | 0.677 | 1.074 | 1.381 | 0.680 | 1.073 | 1.381 |
| 1 | 0.532 | 0.863 | 1.121 | 0.534 | 0.863 | 1.121 |

of the PEST case for different values of $\lambda_1$, $B$, $v_w$, Pr and $E$ are shown in Figs. 7, 8, 9, 10 and 11. It is observed that the temperature profile decreases with the increase in $B$ and increases with the increase in $v_w$ and $\lambda_1$. Moreover, the thermal boundary layer thickness reduces with the increase in $B$ while it increases with the increase in $v_w$ and $\lambda_1$ (see Figs. 7, 8 and 9). It is shown in Fig. 10 that an increase in Pr leads to a decrease in the temperature profile and the thermal boundary layer thickness. Physically, if Pr increases, the thermal diffusivity decreases which results in the decrease of energy penetration ability with reduced thermal boundary layers. The results in Fig. 11 demonstrate that the effect of increasing $E$ is to increase the temperature profile and the thermal boundary layer thickness. This behavior of temperature enhancement occurs as the thermal energy is generated in the fluid due to frictional heating. The temperature profiles of the PEST case for different values of $R$ are shown in Fig. 12. It is depicted that the temperature field and the thermal boundary layer thickness increase with the increase in $R$. The temperature profiles for different values of $B$, $\lambda_1$, $v_w$, Pr, $E$ and $R$ in the PEHF case are shown in Figs. 13, 14, 15, 16, 17 and 18. It is observed that the temperature profile and the thermal boundary layer thickness increase with the increase in $\lambda_1$ $v_w$, $E$ and $R$ while both decrease with the increase in $B$ and Pr

Some obtained HAM results of the wall temperature gradient $-\theta'(0)$ for different values of $E$, Pr and $R$ keeping $\lambda_1 = 0$, $B = 0$ and $v_w = 0$ are given in Tables 1, 2 and 3 along with the numerical results obtained by Bidin and Nazar [28]. It can be seen that these results are in very good agreement. Tables 4 and 5

**Table 2** Values of wall temperature gradient $-\theta'(0)$ in the PEST case for different values of $E$, Pr and $R$ keeping $\lambda_1 = 0$, $B = 0$, $v_w = 0$ and $\hbar_1 = \hbar_2 = \hbar$ in comparisons with the results obtained by Bidin and Nazar [28]

| $R$ | Bidin and Nazar [28] | | | Present results (HAM) | | |
|---|---|---|---|---|---|---|
| | $E = 0.2$ | | | $E = 0.2$ | | |
| | Pr = 1 | Pr = 2 | Pr = 3 | Pr = 1 ($\hbar = -0.75$) | Pr = 2 ($\hbar = -0.4$) | Pr = 3 ($\hbar = -0.6$) |
| 0 | 0.862 | 1.306 | 1.688 | 0.863 | 1.306 | 1.639 |
| 0.5 | 0.618 | 0.965 | 1.229 | 0.620 | 0.965 | 1.229 |
| 1 | 0.488 | 0.782 | 1.007 | 0.491 | 0.782 | 1.007 |

**Table 3** Values of wall temperature gradient $-\theta'(0)$ in the PEST case for different values of $E$, Pr and $R$ keeping $\lambda_1 = 0$, $B = 0$, $v_w = 0$ and $\hbar_1 = \hbar_2 = \hbar$ in comparisons with the results obtained by Bidin and Nazar [28]

| $R$ | Bidin and Nazar [28] | | | Present results (HAM) | | |
|---|---|---|---|---|---|---|
| | $E = 0.9$ | | | $E = 0.9$ | | |
| | Pr = 1 | Pr = 2 | Pr = 3 | Pr = 1 ($\hbar = -0.75$) | Pr = 2 ($\hbar = -0.6$) | Pr = 3 ($\hbar = -0.7$) |
| 0 | 0.539 | 0.725 | 0.830 | 0.539 | 0.725 | 0.830 |
| 0.5 | 0.410 | 0.587 | 0.696 | 0.414 | 0.587 | 0.696 |
| 1 | 0.334 | 0.498 | 0.606 | 0.337 | 0.498 | 0.605 |

**Table 4** Values of local skin friction coefficient $C_{f_x}$ for different values of $v_w$ and $\lambda_1$ when $B = 0.4$, Re = 1 and $\hbar_1 = -0.4$

| $v_w$ | $\lambda_1 = 0$ | $\lambda_1 = 0.5$ | $\lambda_1 = 1$ | $\lambda_1 = 1.5$ |
|---|---|---|---|---|
| −0.4 | 1.27879 | 1.07783 | 0.95863 | 0.878043 |
| −0.2 | 1.19107 | 0.988188 | 0.867419 | 0.785317 |
| 0 | 1.10904 | 0.905504 | 0.784191 | 0.7015 |
| 0.2 | 1.03273 | 0.829822 | 0.70904 | 0.626751 |
| 0.4 | 0.962047 | 0.760982 | 0.641737 | 0.560762 |

**Table 5** Values of local skin friction coefficient $C_{f_x}$ for different values of $v_w$ and $B$ when $\lambda_1 = 0.2$, Re = 1 and $\hbar_1 = -0.4$

| $v_w$ | $B = 0$ | $B = 0.4$ | $B = 0.8$ | $B = 1.2$ |
|---|---|---|---|---|
| −0.4 | 0.970749 | 1.18324 | 1.3472 | 1.48563 |
| −0.2 | 0.895728 | 1.0947 | 1.25432 | 1.39268 |
| 0 | 0.827093 | 1.01239 | 1.16715 | 1.30313 |
| 0.2 | 0.76472 | 0.936349 | 1.0857 | 1.21886 |
| 0.4 | 0.708339 | 0.866449 | 1.00986 | 1.13981 |

**Table 6** Values of local Nusselt number $Nu_x$ in the PEST case for different values of $v_w$ and $E$ when $\lambda_1 = 0.2$, Pr = 2, $B = 0.4$, $R = 0.5$, $\hbar_1 = \hbar_2 = -0.4$ and Re = 1

| $v_w$ | $E = 0$ | $E = 0.5$ | $E = 1$ | $E = 1.5$ |
|---|---|---|---|---|
| −0.4 | 2.33477 | 1.7265 | 1.11822 | 0.509951 |
| −0.2 | 2.07966 | 1.54052 | 1.00139 | 0.462251 |
| 0 | 1.84514 | 1.37042 | 0.895696 | 0.420972 |
| 0.2 | 1.63295 | 1.21764 | 0.802333 | 0.387025 |
| 0.4 | 1.44456 | 1.08348 | 0.722394 | 0.361311 |

**Table 7** Values of local Nusselt number $Nu_x$ in the PEST case for different values of $R$ and $Pr$ when $\lambda_1 = 0.2$, $v_w = 0.2$, $B = 0.4$, $E = 0.5$, $\hbar_1 = \hbar_2 = -0.4$ and Re = 1

| $R$ | Pr = 1 | Pr = 1.5 | Pr = 2 | Pr = 2.5 |
|---|---|---|---|---|
| 0 | 0.669281 | 0.811776 | 0.922358 | 1.00998 |
| 0.5 | 0.852743 | 1.05317 | 1.21764 | 1.35376 |
| 1 | 0.985286 | 1.22863 | 1.43542 | 1.61153 |
| 1.5 | 1.08958 | 1.36633 | 1.60741 | 1.81715 |
| 2 | 1.15195 | 1.45288 | 1.71936 | 1.95436 |

are used to show the values of local skin friction coefficient for various values of $v_w$, $\lambda_1$ and $B$. It is shown that local skin friction coefficient decreases with the increase in $v_w$ and $\lambda_1$ and increases with the increase in $B$. Tables 6 and 7 are made to calculate the values of local Nusselt number $Nu_x$ in the PEST case for different values of $v_w$, $E$, Pr and $R$ It is observed that local Nusselt number $Nu_x$ decreases with the increase in both $v_w$ and $E$ while $Nu_x$ increases with the increase in Pr and $R$.

## 5 Conclusions

A mathematical analysis is carried out for momentum and heat transfer in a boundary layer flow of a Jeffrey fluid over an exponentially stretching porous sheet. Highly nonlinear partial differential equations are converted into ordinary differential equations by applying suitable similarity transformations. Analytical solutions for the velocity and temperature profiles are obtained using homotopy analysis method (HAM).

The main points of the present analysis are summarized as follows:

1. The influence of $\lambda$ on the velocity and temperature profiles is opposite to that of B.
2. The effect of $v_w$ on the velocity and temperature profiles is similar.
3. The results of the PEST cases are qualitatively similar to that of the PEHF cases.
4. The influence of E and R on the temperature profile and thermal boundary layer thickness are quite opposite to that of the Pr.
5. The local skin friction coefficient $C_{f_x}$ is a decreasing function of $v_w$ and $\lambda$ while an increasing function of B.
6. The local Nusselt number $Nu_x$ is a decreasing function of E and $v_w$ while an increasing function of Pr and R.
7. The limiting cases of the results of the paper when $\lambda = 0$, $B = 0$ and $v_w = 0$ are in good agreement with the results of Bidin and Nazar [28].

## References

1. Liu, C.: Flow and heat transfer of an electrically conducting fluid of second grade over a stretching sheet subject to a transverse magnetic field. Int. J. Heat Mass Transfer **47**, 4427–4437 (2004)
2. Abel, S., Veena, P.H., Rajagopal, K., Pravin, V.K.: Non-Newtonian magnetohydrodynamic flow over a stretching surface with heat and mass transfer. Int. J. Non-Linear Mech. **39**, 1067–1078 (2004)
3. Khan, S.K., Abel, M.S., Sonth, R.M.: Viscoelastic MHD flow, heat and mass transfer over a porous stretching sheet with dissipation of energy and stress work. Int. J. Heat Mass Transfer **40**, 47–57 (2003)
4. Cortell, R.: Effects of viscous dissipation and work done by deformation on the MHD flow and heat transfer of a viscoelastic fluid over a stretching sheet. Phys. Lett. A **357**, 298–305 (2006)
5. Liu, C., Anderson, H.I.: Heat transfer in a liquid film on an unsteady stretching sheet. Int. J. Therm. Sci. **47**, 766–772 (2008)

6. Dandapat, B.S., Santra, B., Vajravelu, K.: The effects of variable fluid properties and thermocapillarity on the flow of a thin film on an unsteady stretching sheet. Int. J. Heat Mass Transfer **50**, 991–996 (2007)
7. Nadeem, S., Hussain, A., Malik, M.Y., Hayat, T.: Series solutions for the stagnation flow of a second-grade fluid over a shrinking sheet. Appl. Math. Mech.-Engl. Ed. **30**, 1255–1262 (2009)
8. Abbas, Z., Hayat, T.: Radiation effects on MHD flow in a porous medium. Int. J. Heat Mass Transfer **51**, 1024–1033 (2008)
9. Nadeem, S., Hussain, A.: Stagnation flow of a Jeffrey fluid over a shrinking sheet. Z. N. A **65a**, 1–9 (2010)
10. Nadeem, S., Hussain, A.: MHD flow of a viscous fluid on a non linear porous shrinking sheet with HAM. Appl. Math. Mech.-Engl. Ed. **30**, 1–10 (2009)
11. Nadeem, S., Abbasbandy, S., Hussain, M.: Series solutions of boundary layer flow of a Micropolar fluid near the stagnation point towards a shrinking sheet. Z. N. A **64a**, 575–582 (2009)
12. Nadeem, S., Awais, M.: Thin film flow of an unsteady shrinking sheet through porous medium with variable viscosity. Phys. Lett. A. **372**, 4965–4972 (2008)
13. Sajid, M., Hayat, T.: Influence of thermal radiation on the boundary layer flow due to an exponentially stretching sheet. Int. Commun. Heat Mass Transf. **35**, 347–356 (2008)
14. Sanjayanand, E., Khan, S.K.: On heat and mass transfer in a viscoelastic boundary layer flow over an exponentially stretching sheet. Int. J. Therm. Sci. **45**, 819–828, (2006)
15. Khan, S.K., Sanjayanand, E.: Viscoelastic boundary layer flow and heat transfer over an exponential stretching sheet. Int. J. Heat Mass Transfer **48**, 1534–1542 (2005)
16. Magyari, E., Keller, B.: Heat and mass transfer in the boundary layer on an exponentially stretching continuous surface. J. Phys. D: Appl. Phys. **32**, 577–785 (1999)
17. Hayat, T., Sajid, M.: Homotopy analysis of MHD boundary layer flow of an upper-convected Maxwell fluid. Int. J. Eng. Sci. **45**, 393–401 (2007)
18. Liao, S.J.: Beyond Perturbation: Introduction to Homotopy Analysis Method. Chapman & Hall/CRC, Boca Raton (2003)
19. Liao, S.J.: Notes on the Homotopy analysis method: some definitions and theorems. Comm. Nonlinear Sci. Numer. Simul. **14**, 983–997 (2009)
20. Liao, S.J.: On the Homotopy analysis method for nonlinear problems. Appl. Math. Comput. **147**, 499–513 (2004)
21. Liao, S.J.: Finding multiple solutions of nonlinear problems by means of the Homotopy analysis method. J. Hydrodynam. Ser. B **18**, 54–56 (2006)
22. Nadeem, S., Ali, M.: Analytical solutions for pipe flow of a fourth grade fluid with Reynold and Vogel's models of viscosities. Comm. Nonlinear Sci. Numer. Simul. **14**, 2073–2090, (2009)
23. Nadeem, S., Hussain, A., Khan, M.: HAM solutions for boundary layer flow in the region of the stagnation point towards a stretching sheet. Comm. Nonlinear Sci. Numer. Simul. **15**, 475–481 (2010)
24. Abbasbandy, S., Hayat, T.: Solution of the MHD Falkner–Skan flow by Homotopy analysis method. Comm. Nonlinear Sci. Numer. Simul. **14**, 3591–3598 (2009)
25. Abbasbandy, S.: Homotopy analysis method for heat radiation equations. Int. Comm. Heat Mass Transfer **34**, 380–387 (2007)
26. Abbasbandy, S.: The application of Homotopy analysis method to solve a generalized Hirota–Satsuma coupled KDV equation. Phys. Lett. A **361**, 478–483 (2007)
27. Abbasbandy, S., Samadian, Z.F.: Soliton solutions for the fifth-order KDV equation with Homotopy analysis method. Nonlinear Dyn. **5**, 183–187 (2008)
28. Bidin, B., Nazar, R.: Numerical solution of the boundary layer flow over an exponentially stretching sheet with thermal radiation. Eur. J. Sci. Res. **33**, 710–717 (2009)